

Title	The parsec-scale radio jet of BL Lac
Authors	Gabuzda, Denise;Cawthorne, T. V.
Publication date	2003
Original Citation	Gabuzda, D. C. and Cawthorne, T. V. (2003) 'The parsec-scale radio jet of BL Lac', Monthly Notices of the Royal Astronomical Society, 338(2), pp. 312-322. doi: 10.1046/j.1365-8711.2003.06034.x
Type of publication	Article (peer-reviewed)
Link to publisher's version	<a href="https://academic.oup.com/mnras/article-lookup/doi/10.1046/j.1365-8711.2003.06034.x">https://academic.oup.com/mnras/article-lookup/doi/10.1046/j.1365-8711.2003.06034.x</a> - <a href="https://doi.org/10.1046/j.1365-8711.2003.06034.x">10.1046/j.1365-8711.2003.06034.x</a>
Rights	© 2003, Royal Astronomical Society
Download date	2024-05-06 17:28:44
Item downloaded from	<a href="https://hdl.handle.net/10468/4990">https://hdl.handle.net/10468/4990</a>

# The parsec-scale radio jet of BL Lac

D. C. Gabuzda<sup>1,2\*</sup>† and T. V. Cawthorne<sup>3</sup>

<sup>1</sup>*Joint Institute for VLBI in Europe, Postbus 2, 7990 AA Dwingeloo, the Netherlands*

<sup>2</sup>*Astro Space Centre, P.N. Lebedev Physical Institute, Leninsky Prospekt 53, 117924, Moscow, Russia*

<sup>3</sup>*Centre for Astrophysics, University of Central Lancashire, Preston, Lancashire, PR1 2HE*

Accepted 2002 September 3. Received 2002 August 29; in original form 2002 July 9

## ABSTRACT

Polarization-sensitive  $\lambda = 6$  cm global VLBI images of BL Lac for data taken at three epochs are presented and analysed, together with an additional epoch for which only total intensity data are available. Previous  $\lambda = 6$  cm and  $\lambda = 3.6$  cm VLBI polarization observations of BL Lac have shown that the jet components in this source tend to have magnetic field transverse to the jet direction. On the whole, these images confirm this tendency, though there is evidence for possibly oblique or longitudinal magnetic fields in some features at some epochs. The flux densities of individual features moving from the core can initially drop rapidly, but the rate of flux decrease slows with time, so that many features are, in fact, remarkably long-lived. This has made it possible to trace the movements of some components over more than a decade. The trajectories of individual components show oscillations whose amplitude appears to grow with distance from the VLBI core.

**Key words:** polarization – BL Lacertae objects: general – BL Lacertae objects: individual: BL Lac – radio continuum: galaxies.

## 1 INTRODUCTION

BL Lacertae objects are extragalactic sources displaying weak, sometimes undetectable, line emission and strong and variable polarization in wavebands ranging from optical through radio. Usually, they have compact, flat-spectrum radio structure, and point-like optical structure; for some, luminous elliptical host galaxies are observed (Angel & Stockman 1980; Miller 1981; Kollgaard 1994). The radio emission and much of the optical emission is believed to be synchrotron radiation.

BL Lac itself – the prototype of the class – was originally known as a variable star, and was identified with the radio source VRO 42.22.01 by Schmidt (1968). It lies at the centre of a giant elliptical galaxy at a redshift of 0.069 (Miller, French & Hawley 1978; Vermeulen et al. 1995). After more than two decades of observations in which its spectrum was essentially featureless, the spring 1995 observations of Vermeulen et al. showed clearly visible broad H $\alpha$  emission, together with emission from several less prominent lines. This emergence of line emission could not be accounted for by variation of the continuum level alone, indicating variability in the actual broad line flux by a factor of five or more within six years (Vermeulen et al. 1995), the origin of which is not clear.

BL Lac is violently variable in the optical and infrared, significant changes in brightness and polarization occurring on time-scales as

short as a day (Brindle et al. 1985; Impey et al. 1984). The degree of optical polarization is  $\sim 5$ –20 per cent, and there is evidence for a preferred optical polarization position angle in the range  $\sim 10^\circ$ – $40^\circ$  (Angel & Stockman 1980; Brindle et al. 1985; Sitko, Schmidt & Stein 1985; Smith et al. 1987). Impey et al. (1984) observed the infrared polarization to be erratic, though the position angle was comparatively stable at  $\chi \simeq 10^\circ$ . There is no obvious correlation between optical and radio variations (Pomphrey et al. 1976), but the preferred direction for the infrared and optical polarization roughly coincides with the direction of the VLBI jet on scales of  $\sim 1$ –3 mas.

BL Lac is highly variable at radio wavelengths on time-scales as short as a few days; the radio polarization is comparatively high, varying from  $\sim 0$ –10 per cent (Altschuler & Wardle 1976; Aller et al. 1985). VLA maps by Antonucci et al. (1986) and Kollgaard et al. (1992) reveal the source to be very compact; the only arcsecond-scale structure is an extended halo-like structure with angular extent  $\sim 40$  arcmin. A series of flux and polarization outbursts in  $\sim 1980$ –1984 have been successfully fit with models in which a ‘piston’ drives plane shocks down a relativistic jet (Hughes, Aller & Aller 1989).

Previous VLBI maps show structure along position angle  $\sim 190^\circ$ , and superluminal motions in this direction have been reported for a number of components (Mutel et al. 1990; Denn et al. 2000). Previous VLBI polarization images at centimetre wavelengths (Gabuzda, Wardle & Roberts 1989; Cawthorne et al. 1993) have shown that the jet polarization vectors (i.e.  $E$  vectors) are aligned with the jet direction, as is typical for BL Lacertae objects (Gabuzda, Pushkarev & Cawthorne 2000).

\*E-mail: gabuzda@phys.ucc.ie

†Present address: Physics Department, University College Cork, Cork, Ireland.

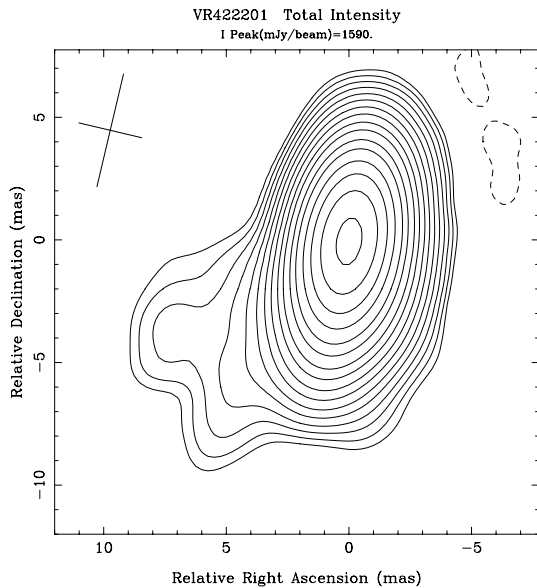


**Figure 1.** VLBI  $I$  image of BL Lac at epoch 1986.45, with contours at  $-0.5, 0.5, 0.7, 1.0, 1.4, 2.0, 2.8, 4.0, 5.6, 8.0, 11.3, 16.0, 22.6, 32.0, 45.2, 64.0,$  and  $90.5$  per cent of the peak brightness of  $1.59 \text{ Jy beam}^{-1}$ .

The images presented here complement the higher-frequency VLBI study of Denn et al. (2000). In some of these more recent 2- and 1.3-cm images, the VLBI jet bends toward the east or west several mas from the core. Denn et al. (2000) model the inner sections of these bends using helical jet trajectories. In the time range covered by our 6-cm images, which have lower resolution but detect emission further from the core, we can clearly see a sharp bend toward the east in the images. Unlike Denn et al. (2000), we have been able to follow several components well after they have flowed past this bend.

We assume throughout a Friedmann universe with Hubble constant of  $100 h \text{ km s}^{-1} \text{ Mpc}^{-1}$  and  $q_0 = 0.5$ .

## 2 OBSERVATIONS

We present here new 6-cm total intensity images of BL Lac for epoch 1986.45 (Fig. 1), and total intensity and polarization images at three epochs from 1987.41–1992.23 (Figs 2 to 4). In addition, we have reanalysed the VLBI polarization images previously published by Gabuzda et al. (1989) and Cawthorne et al. (1993), since the software for modelling the polarized visibility data has significantly improved since the earlier results were obtained. Table 1 shows a summary of the antennas and observing frequencies for each of the six epochs analysed here. All observations were made under the auspices of the US and European VLBI networks. In each case, the data were recorded using the Mk III VLBI system and correlated on the Mk IIIA correlator at Haystack Observatory.

The calibration of these data was performed as described by Roberts, Wardle & Brown (1994). Hybrid maps of the distribution of total intensity  $I$  were made using a self-calibration algorithm similar to that described by Cornwell & Wilkinson (1981). Maps of the distribution of linear polarization<sup>1</sup>  $P$  were made by referencing

<sup>1</sup>  $P = pe^{2ix} = mle^{2ix}$ , where  $p = ml$  is the polarized intensity,  $m$  is the fractional linear polarization, and  $\chi$  is the position angle of the electric vector on the sky.

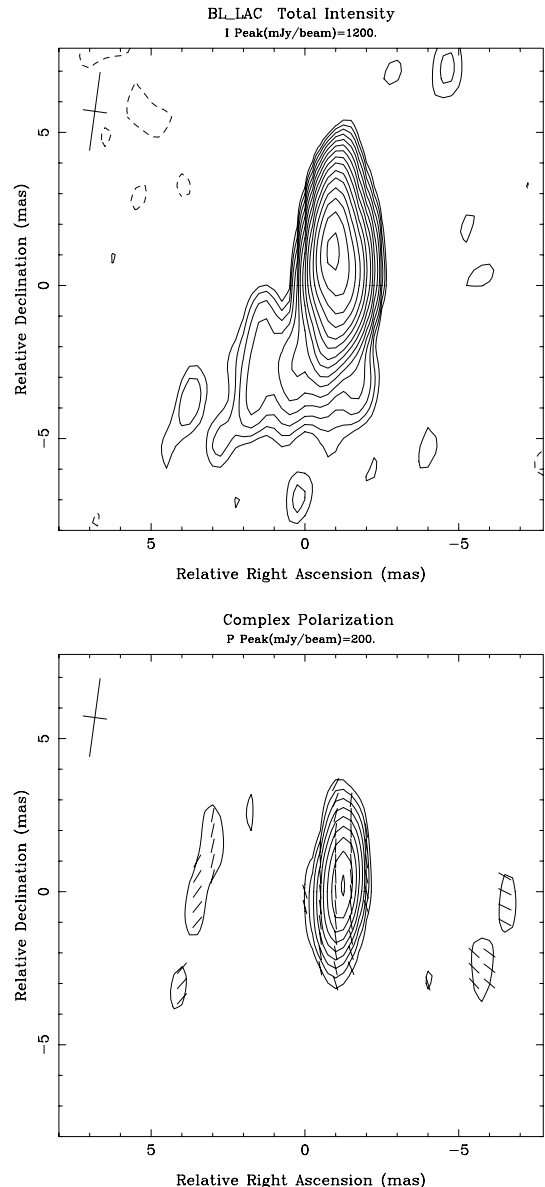


**Figure 2.** VLBI images of BL Lac at epoch 1987.41: (a)  $I$ , with contours at  $-0.7, 0.7, 1.0, 1.4, 2.0, 2.8, 4.0, 5.6, 8.0, 11.3, 16.0, 22.6, 32.0, 45.2, 64.0,$  and  $90.5$  per cent of the peak brightness of  $1.20 \text{ Jy beam}^{-1}$ . (b)  $P$ , with contours of polarized intensity at  $6.0, 8.5, 12.0, 17.0, 24.0, 34.0, 48.0, 68.0,$  and  $96.0$  per cent of the peak brightness of  $200.0 \text{ mJy beam}^{-1}$ , and  $\chi$  vectors superimposed.

the cross-hand fringes to the parallel-hand fringes using the antenna gains determined in the hybrid mapping, Fourier transforming the cross-hand fringes, and performing a complex CLEAN. In this way, registration of the  $I$  and  $P$  maps to within a small fraction of a fringe spacing is assured.

## 3 RESULTS

In each of the images (Figs 1 to 4), the restoring beam is shown as a cross in a corner of the image. For the linear polarization maps, the contours are those of polarized intensity  $p$ , and the plane of the electric vector  $\chi$  is indicated by the sticks that are superimposed. There is always the possibility that the observed polarization

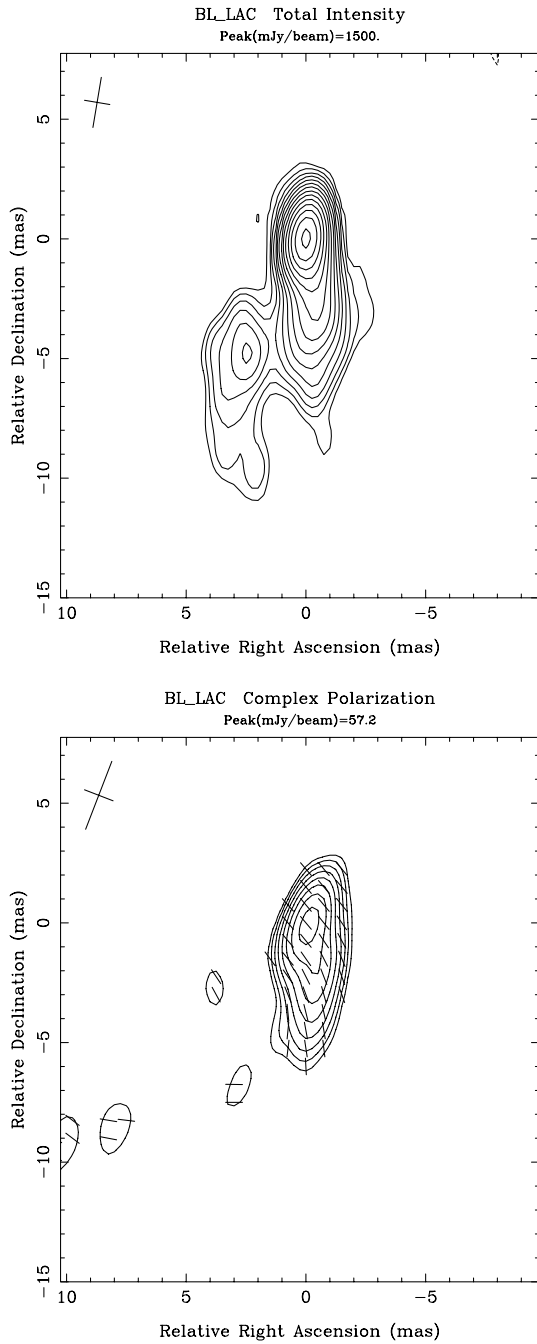


**Figure 3.** VLBI images of BL Lac at epoch 1990.88: (a)  $I$ , with contours at  $-1.0, 1.0, 1.4, 2.0, 2.8, 4.0, 5.6, 8.0, 11.3, 16.0, 22.6, 32.0, 45.2, 64.0,$  and  $90.5$  per cent of the peak brightness of  $1.50 \text{ Jy beam}^{-1}$ . (b)  $P$ , with contours of polarized intensity at  $7.5, 10.6, 15.0, 21.2, 30.0, 42.5, 60.0, 85.0$  per cent of the peak brightness of  $58.8 \text{ mJy beam}^{-1}$ , and  $\chi$  vectors superimposed.

position angles include some contribution due to Faraday rotation along the line of sight to the emission region. Rudnick & Jones (1983) determined the integrated rotation measure for BL Lac to be comparatively large,  $-205 \text{ rad m}^{-2}$ , implying a rotation of  $-42^\circ$  at 6 cm. Rudnick et al. (1984) confirmed this result, and suggested that the rotation measure is constant in time and is due primarily to our Galaxy. Simultaneous, multi-wavelength VLBA observations have verified the presence of a constant foreground Faraday screen along the lines of sight to several distinct VLBI jet components, with a very different rotation measure indicated for the VLBI core (Reynolds,

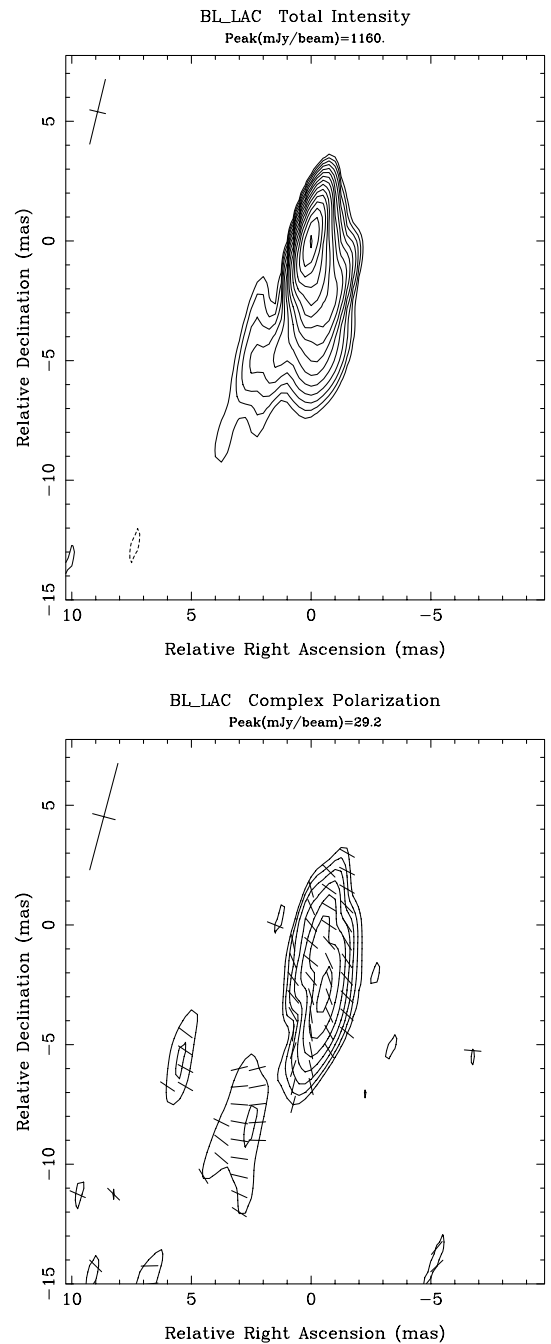


**Figure 4.** VLBI images of BL Lac at epoch 1992.23: (a)  $I$ , with contours at  $-0.75, 0.75, 1.1, 1.5, 2.1, 3.0, 4.2, 6.0, 8.5, 12.0, 17.0, 24.0, 34.0, 48.0, 68.0,$  and  $96.0$  per cent of the peak brightness of  $1.16 \text{ Jy beam}^{-1}$ . (b)  $P$ , with contours of polarized intensity at  $11.0, 15.6, 22.0, 31.1, 44.0, 62.2,$  and  $88.0$  per cent of the peak brightness of  $29.2 \text{ mJy beam}^{-1}$ , and  $\chi$  vectors superimposed.

Cawthorne & Gabuzda 2001). However, the best estimate of the foreground rotation measure is  $-108 \text{ rad m}^{-2}$ , suggesting that the integrated rotation measure determined by Rudnick et al. (1984) may have been affected by intrinsic Faraday rotation near the core, so that it did not accurately reflect the foreground (Galactic) rotation measure. We believe, therefore, that the best estimate of the foreground rotation measure is given by the results of Reynolds et al. (2001), based on simultaneous, multi-frequency VLBI polarization measurements. Note, however, that this result must be verified; in

addition, we cannot rule out the possibility that the foreground rotation measure changed between the measurements of Rudnick et al. (1984) and those of Reynolds et al. (2001). We have used the new foreground rotation measure estimate of Reynolds et al. (2001) to correct all the  $\chi$  values in the polarization images and in Figs 6 to 11 (later), but list  $\chi_0$  values corresponding to both proposed foreground rotation measures in Table 2 for completeness.

Models for the source structures were derived by fitting the complex  $I$  and  $P$  visibilities that come from the imaging process as described by Roberts, Gabuzda & Wardle (1987) and Gabuzda et al. (1989). The model fits are shown in Table 2. In all cases, the  $I$  and  $P$  visibilities were fitted separately, in order to allow for small differences in the positions and sizes of corresponding  $I$  and  $P$  components, either intrinsic to the source structure or associated with residual calibration errors. When  $P$  components have been identified with specific  $I$  components, their positions agree to within a quarter of a beam width or less. The errors on  $r$  in Table 2 are formal  $1\sigma$  errors, corresponding to an increase in the best-fitting  $\chi^2$  by unity. The smallest of these formal errors almost certainly underestimate the actual errors; realistically, the smallest  $1\sigma$  errors in component separations are probably no less than  $\sim 0.05$  mas.

In each of the total intensity images, the jet initially emerges from the core in position angle  $\sim -170$ , then turns sharply toward the east. The jet structure is fairly complex; we have modelled it using the circular Gaussian components in Table 2. When determining how many components to use for a particular data set, we added components only if there was clear evidence for them from the distribution of CLEAN components, and if adding them significantly decreased the  $\chi^2$  for the fit.

At first glance, the total-intensity images do not seem to show dramatic structural changes. Inspection of the models in Table 2 indicates that, in the first four epochs analysed here, the strongest feature in the images is not the northernmost feature, i.e. the 6-cm core. This was also the case in a number of epochs analysed by Mutel et al. (1990). The fact that we clearly detected polarization from the weaker, northernmost feature at epochs 1984.23 and 1987.41 gives us confidence that this feature is the core and not a mapping artefact. At epochs 1990.88 and 1992.23, however, the northernmost feature detected in our images is the brightest component, suggesting that the core was undergoing an outburst at that time.

Our model fitting, based on the distributions of CLEAN components, indicates that individual features travelling along the jet can

experience rapid flux changes, especially when they are ‘young’ and close to the core. Further from the core, their flux evolution slows substantially, so that, in the end, they are remarkably long-lived.

The polarization of individual components can also change very rapidly. This is clear even from a visual inspection of the three  $P$  images in Figs 2–4: the  $P$  peak drops from 200 mJy to 29 mJy over about five years. Our models in Table 2 show that this is primarily owing to changes in the polarized fluxes of components in the inner VLBI jet.

#### 4 ANALYSIS OF TOTAL INTENSITY IMAGES

Fig. 5 shows a plot of separation from the core versus epoch for all jet components detected in the 2.8-, 3.6-, and 6-cm images analyzed by Mutel et al. (1990), Gabuzda & Cawthorne (1996), and this paper. It is obvious that this plot does not represent a set of jet features moving uniformly from the core at constant speed, though there are clearly segments corresponding to individual components separating from the core at nearly constant speed. In addition, there are several cases in which the measurements of Mutel et al. (1990) and our own measurements at nearby epochs are quite consistent, increasing our confidence in the value of performing an analysis taking into account all the available data.

We will now use the collected model-fitting results to identify measurements corresponding to individual jet features in this plot, in order to study their evolution as they move outward. The value of the 6-cm images presented here is immediately evident: they make it possible to follow the jet much further from the core. When identifying components across epochs, we have tried to join position measurements at different epochs as smoothly as possible and leave as few components unaccounted for as possible, taking into account both the information in Fig. 5 and the implied trajectories of proposed components in the plane of the sky (Figs 6–11). We summarize our estimates of superluminal speeds  $\beta_{app}$  ( $\beta = v/c$ ) for the four components for which the most data are available in Table 3. These speeds are modest,  $\beta_{app} \simeq 1.5$ – $3.5$ , as has generally been found in previous VLBI studies of BL Lac.

##### 4.1 Component S1/K1

Based on the location of its points in Fig. 5, we tentatively identified the feature we have labelled K1 in Table 2 with component S1 of

**Table 1.** Antennas used.

Antenna	Location	Diameter (m)	1984.23	1984.78	1986.45	1987.41	1990.88	1992.23
N	Noto, Italy	32					X	
L	Bologna, Italy	32				X	X	X
B	Bonn, Germany	100	X	X	X	X	X	X
W	WSRT, Netherlands	$\sqrt{14} \times 25$				X	X	
J	Jodrell Bank, UK						X	
K	Westford, MA	37	X	X	X	X	X	X
G	Green Bank, VA	43	X	X	X	X	X	X
I (VLBA)	North Liberty, IO	25						X
F	Fort Davis, TX	26	X	X	X	X		
F (VLBA)	Fort Davis, TX	25					X	X
X (VLBA)	Los Alamos, NM	25						X
Y <sub>27</sub>	Socorro, NM	$\sqrt{27} \times 25$	X	X	X	X	X	X
P (VLBA)	Pietown, NM	25						X
O	Big Pine, CA	40	X	X	X	X	X	
O (VLBA)	Big Pine, CA	25						X

**Table 2.** Models for BL Lac.

Comp.	$I$ (mJy)	$p$ (mJy)	$\chi_0$ (deg) <sup>a</sup>	$\chi_0$ (deg) <sup>b</sup>	$m$ (per cent)	$r$ (mas) <sup>c</sup>	$\Delta r$ (mas)	PA (deg) <sup>c</sup>	$\Delta$ PA (deg)	FWHM (mas)
1984.23										
C	323	15.3	115	95	4.7	...	...	...	...	0.11
K3	1261	48.0	1	-19	3.8	1.31	0.03	184	1.8	0.37
K2	780	50.2	4	-16	6.4	2.68	0.04	181	1.0	0.67
K	230	12.2	-14	-34	5.3	5.41	0.08	171	1.4	1.55
1984.78										
C	249	<14	...	...	<5.6	...	...	...	...	0.12
K3	1270	50.8	+45	+25	4.0	1.46	0.02	181	1.0	0.52
K2	907	115.4	+25	+5	12.7	2.74	0.02	185	0.6	0.44
K1	310	33.9	-48	-68	10.9	3.93	0.03	170	0.5	0.41
1986.45										
C	377	-	-	-	-	...	...	...	...	1.17
K5	916	-	-	-	-	1.16	0.05	154	1.9	0.65
K3	370	-	-	-	-	2.20	0.08	177	1.1	0.02
K2	185	-	-	-	-	3.32	0.06	-170	1.4	0.73
K1	166	-	-	-	-	4.72	0.14	160	1.4	2.34
1987.41										
C	323	23.5	-25	-45	7.2	...	...	...	...	0.22
K5	1211	93.2	+16	-4	7.7	1.36	0.03	183	0.6	0.42
K3	514	138.3	+24	+4	26.9	2.45	0.05	195	0.6	0.02
K2	263	42.4	+62	+42	16.1	3.53	0.05	181	0.8	0.67
K1	114	33.6	-39	-59	29.5	5.76	0.19	166	2.3	1.66
1990.88										
C	1402	56.3	+68	+48	4.0	...	...	...	...	0.09
K7	222	<4	...	...	<1.8	1.09	0.04	-160	1.8	0.24
K6	171	20.2	+63	+43	11.8	1.56	0.10	-174	3.2	0.98
K5	272	22.5	+27	+7	8.3	2.94	0.06	-167	0.5	0.84
K3	225	13.8	+32	+12	6.1	4.63	0.08	-177	0.6	1.46
K2	154	2.8	+2	-18	1.8	5.12	0.08	152	0.6	1.12
K1	49	<4	...	...	<8.2	7.42	0.20	155	1.3	1.22
K	57	<4	...	...	<7.0	9.74	0.22	161	1.0	1.39
1992.23										
C	1148	15.9	+12	-8	1.4	...	...	...	...	0.21
K7	201	15.1	+88	+68	7.5	1.10	0.04	-166	2.1	0.06
K	300	47.5	+84	+64	16.5	2.11	0.03	-172	0.7	0.83
K6	163	<3	...	...	<1.9	2.38	0.03	-155	0.5	0.86
K5	81	5.4	-19	-39	6.7	4.45	0.07	172	0.6	1.41
K	50	4.6	-24	-44	9.2	4.78	0.10	163	1.1	1.60
K3	108	15.3	+44	+24	14.2	4.92	0.04	-175	0.3	1.07
K2	50	8.1	-31	-51	16.2	5.68	0.15	152	1.5	1.71
K1	63	5.0	+80	+60	8.0	9.14	0.17	159	1.0	2.74

<sup>a</sup>Corrected for a foreground rotation measure of  $-205 \text{ rad m}^{-2}$  (Rudnick et al. 1984).

<sup>b</sup>Corrected for a foreground rotation measure of  $-108 \text{ rad m}^{-2}$  (Reynolds et al. 2001), our preferred value.

<sup>c</sup>Separations and position angles with respect to C.

Mutel et al. (1990). Fig. 6(a) shows a plot of the separation from the core versus epoch for S1/K1, and Fig. 6(b) shows the corresponding trajectory on the sky. The epochs for measurements at 6 cm are indicated next to each of the filled triangles. We can see that the early measurements of Mutel et al. (1990) and our later measurements can be smoothly joined in a natural way; the slightly curved path of S1/K1 on the sky corresponds to the gentle deviations from a straight line (corresponding to constant speed along a constant direction) in Fig. 6(a). For these reasons, we feel confident that our component K1 should be identified with S1; although the sensitivity of subsequent 2.8-cm observations of Mutel et al. (1990) was not sufficient to detect this feature further than about 2 mas from the core, our 6-cm images are able to follow it out to substantially greater distances.

Note here that, looking at Fig. 5, one might be initially tempted to join the earlier measurements for S2 with our measurements for K1. This would yield a reasonable looking linear behaviour for this set of position measurements in Fig. 5. However, in this case, there would be no natural way to join the measurements for our component

K2 with the earlier measurements. This illustrates the fact that, as pointed out above, the identification scheme we have adopted both yields reasonable trajectories for all components and leaves as few component measurements unaccounted for as possible.

Although the trajectory followed by S1/K1 is curved, the increase in its separation from the core in Fig. 6(a) is approximately linear in two intervals, before 1983.0 and after 1984.0. The inferred proper motions in these two intervals are  $1.13$  and  $0.67 \text{ mas yr}^{-1}$ , respectively, corresponding to superluminal speeds  $\beta_{\text{app}}h = 3.51$  and  $2.08$ . As indicated by Fig. 6(b), this change in speed is associated with bending of the jet trajectory.

#### 4.2 Component S2/K2

Moving inward, the feature we have labelled K2 in Table 2 can be clearly identified with component S2 of Mutel et al. (1990). Fig. 7(a) shows a plot of the separation from the core versus epoch for S2/K2, and Fig. 7(b) shows the corresponding trajectory on the sky. Here,

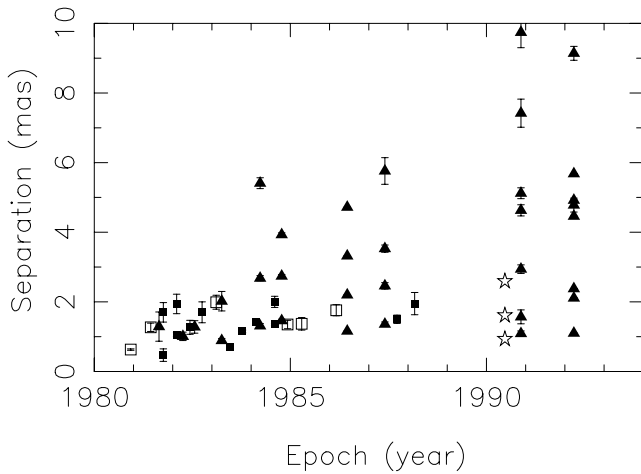


**Figure 5.** Positions of all detected components in the VLBI jet of BL Lac in a plot of separation from the core versus epoch. The filled triangles show 6-cm model-fit results from this paper and from Mutel et al. (1990); the filled squares show 2.8-cm results from Mutel et al. (1990); the hollow squares show 2.8-cm results from Mutel et al. (1990) for images made with 4 or fewer antennas; and the stars show the 3.6-cm results of Gabuzda & Cawthorne (1996). The errors shown are  $2\sigma$ .

the gap between the 6- and 2.8-cm observations of Mutel et al. (1990) and our own 6-cm observations is only about one year, and it is clear that they can be smoothly joined. The deviations from linear behaviour in Fig. 7(a) are somewhat larger, but the collected points still form an only gently curving line. The trajectory on the sky continues to propagate roughly in position angle  $-170^\circ$  until the last three measurements, when it moves sharply to the south-east.

Overall, the behaviour of S2/K2 in Fig. 7(a) is much more regular than one might expect based on its sharply bent trajectory, since the feature on average continues to increase its separation from the core with time. The increase in the separation of S2/K2 from the core is approximately linear in two intervals, with a break in the speed observed at about epoch 1983.5, just before the jet begins to deviate from its initial trajectory. The inferred proper motions in these two intervals are  $1.04 \text{ mas yr}^{-1}$  and  $0.39 \text{ mas yr}^{-1}$ , respectively, corresponding to superluminal speeds  $\beta_{\text{app}}h = 3.23$  and 1.21.

### 4.3 Component K3

The situation with the next component to emerge from the core is less clear. Mutel et al. (1990) identified a feature S3 in their 2.8-cm images at four epochs from 1982.78 to 1984.60, which appeared to have a trajectory on the sky within  $\sim 2$  mas of the core similar to that of S1. They also identified a nearly stationary feature S4 in their 2.8-cm images at four epochs from 1984.60 to 1986.17, which appeared for the first time at a substantial distance from the core (1.35 mas). The relation between these two features is not clear; it seems likely that S4 was actually present but overlooked in the images of Mutel et al. (1990) before they included it in their model fitting. If this is the case, the jet emission in the 2.8-cm model fits of Mutel et al. (1990) for epochs from 1982.78 to 1986.17 actually represents a mixture of S3 and S4, which have not always been accurately separated.

For this reason, we were not able to make plots for our component K3 combining our fits with 6- and 2.8-cm fits for a corresponding feature from the analysis of Mutel et al. (1990). However, we were able to combine our six 6-cm epochs with the 6-cm model fitting

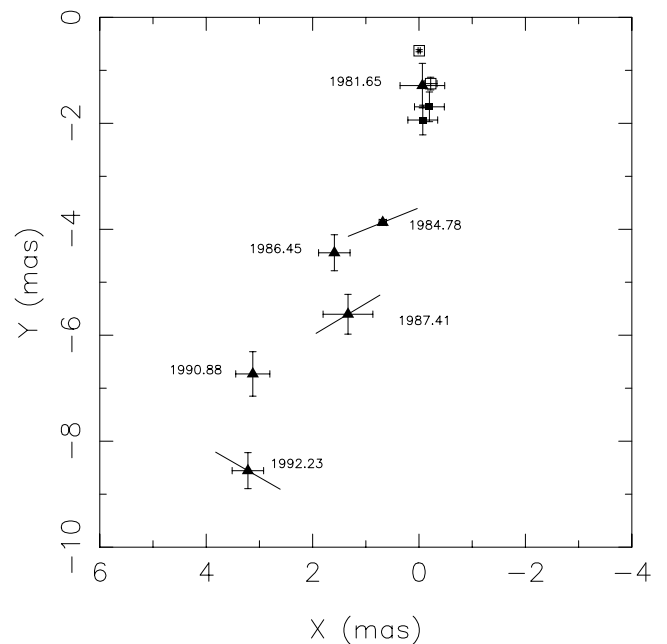
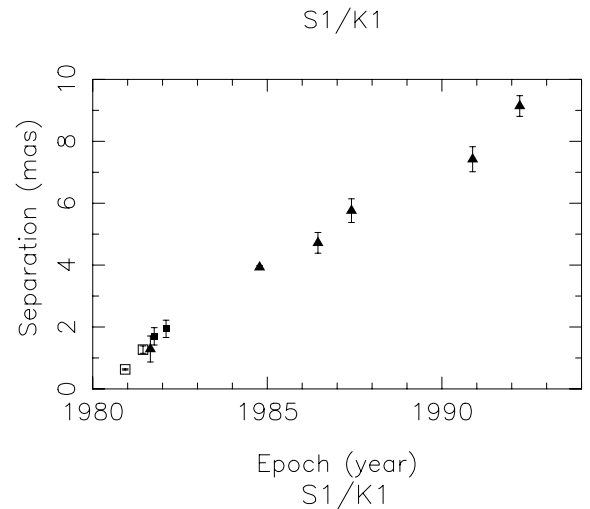


**Figure 6.** (a) Plot of separation from the core versus epoch for our feature K1, identified with component S1 of Mutel et al. (1990). (b) Trajectory on the sky of S1/K1. The meaning of the symbols is the same as in Fig. 5. Epochs for 6-cm measurements are indicated next to each of the filled triangles. When measured, the orientation of  $\chi_0$  is shown by a superposed stick (corrected for a foreground rotation measure of  $-108 \text{ rad m}^{-2}$ ). Errors are  $2\sigma$ .

of Mutel et al. (1990) for epoch 1983.25; the results are shown in Fig. 8.

The behaviour of K3 in Fig. 8(a) is approximately linear throughout the interval for which observations of this component are available. It is natural to think that this may be related to the lack of obvious sharp bending in the trajectory for this component, in contrast to the trajectories of S1/K1 and S2/K2. The inferred proper motion is  $0.48 \text{ mas yr}^{-1}$ , corresponding to the superluminal speed  $\beta_{\text{app}}h = 1.49$ , appreciably lower than for S1/K1 and S2/K2 when they were at comparable distances from the core.

### 4.4 Component S5/K5

Further, it appears we can identify our component K5 with the feature S5 identified by Mutel et al. (1990) and Denn et al. (2000).

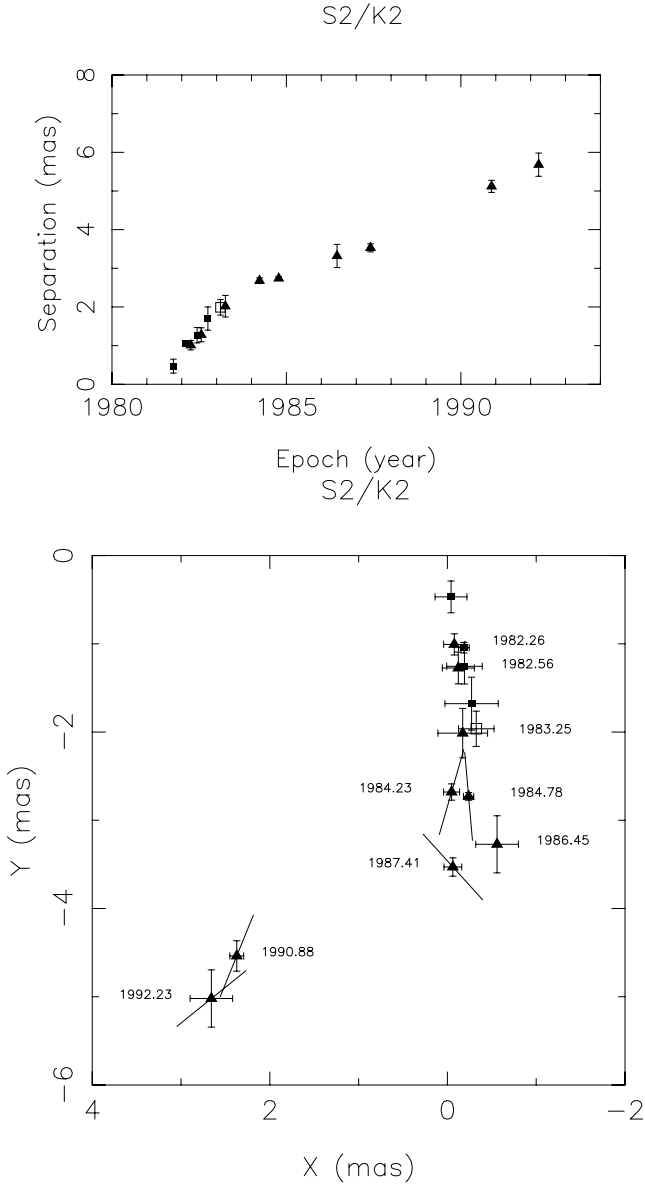


**Figure 7.** (a) Plot of separation from the core versus epoch for our feature K2, identified with component S2 of Mutel et al. (1990). (b) Trajectory on the sky of S2/K2. The meaning of the symbols is the same as in Fig. 5. Epochs for 6-cm measurements are indicated next to each of the filled triangles. When measured, the orientation of  $\chi$  is shown by a superposed stick (corrected for a foreground rotation measure of  $-108 \text{ rad m}^{-2}$ ). Errors are  $2\sigma$ .

Fig. 9(a) shows a plot of the separation from the core versus epoch for S5/K5, and Fig. 9(b) shows the corresponding trajectory on the sky. Assuming that the trajectory originates at the point (0, 0), the inferred trajectory suggests fairly sharp bending of the jet within the first mas or so from the core. There is some evidence for such strong curvature for the trajectories of other features from the higher-resolution images of Denn et al. (2000), and also from the behaviour of S2/K2 several mas from the core. Further, the jet curves toward the south-east, similar to S1/K1 and S2/K2.

As we can see in Fig. 9(b), the last two measurements of this feature were made after the south-eastward bend in the trajectory. Likewise, the corresponding two points in Fig. 9(a) are offset somewhat from the remaining points at earlier epochs, which show an

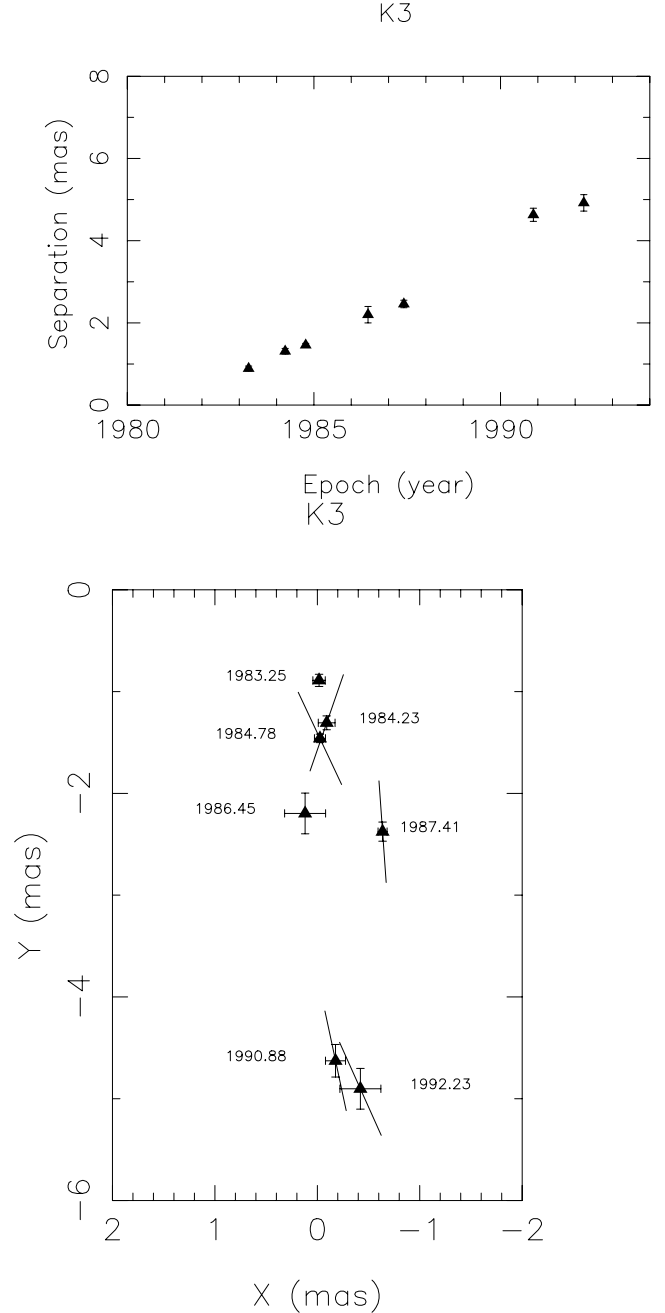


**Figure 8.** (a) Plot of separation from the core versus epoch for our feature K3, together with one 6-cm measurement of Mutel et al. (1990) that can be identified with this component. (b) Trajectory on the sky of K3. Only 6-cm measurements are shown (see text). Epochs are indicated next to each of the points. When measured, the orientation of  $\chi$  is shown by a superposed stick (corrected for a foreground rotation measure of  $-108 \text{ rad m}^{-2}$ ). Errors are  $2\sigma$ .

approximately linear increase in the separation of S5/K5 with time. The inferred proper motion is  $0.48 \text{ mas yr}^{-1}$ , corresponding to the superluminal speed  $\beta_{\text{app}}h = 1.49$ , similar to K3.

#### 4.5 Components K6 and K7

We have measurements for our components K6 and K7 at only three epochs. There is not a clear correspondence between these features

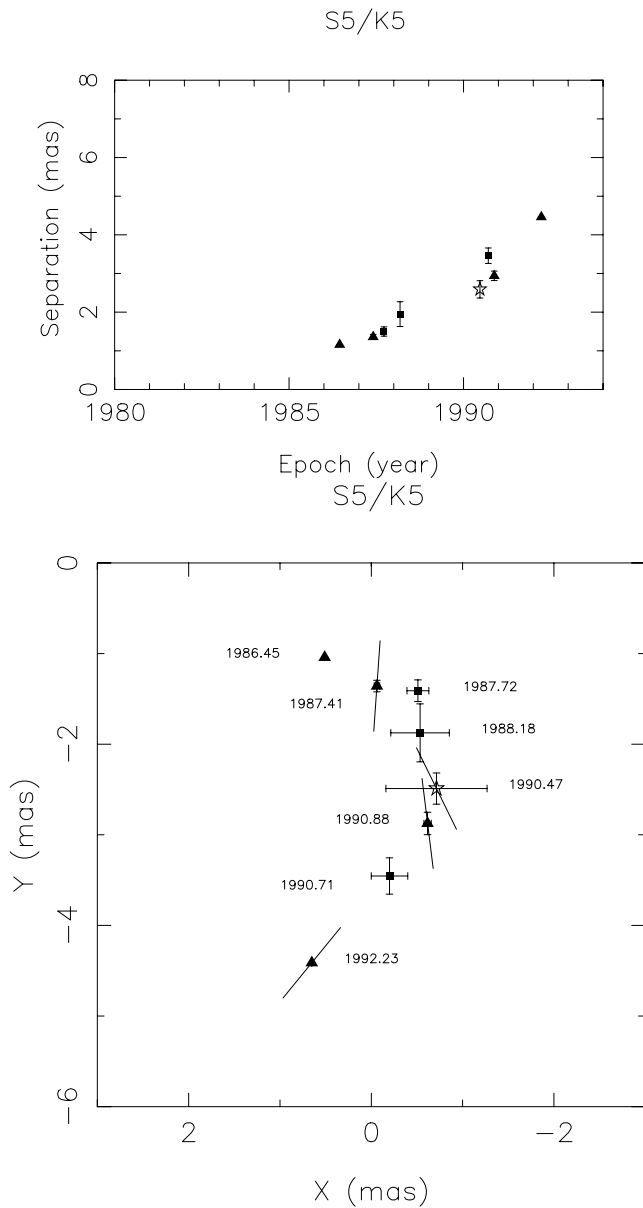


**Figure 9.** (a) Plot of separation from the core versus epoch for our feature K5, identified with component S5 of Mutel et al. (1990). (b) Trajectory on the sky of S5/K5. The meaning of the symbols is the same as in Fig. 5. Epochs are indicated next to each of the points. When measured, the orientation of  $\chi$  is shown by a superposed stick (corrected for a foreground rotation measure of  $-108 \text{ rad m}^{-2}$ ). Errors are  $2\sigma$ .

and higher frequency components identified by Denn et al. (2000), which is not entirely surprising given the difference in frequency for the two sets of observations. Their separation from the core and trajectories are shown in Figs 10 and 11. Our measurements only cover the first  $\sim 2$  mas from the core, and are consistent (within the errors) with straight or only gently curving trajectories for these components in this region.

#### 4.6 Component trajectories in BL Lac

Our analysis indicates a number of important observational facts about the behaviour of trajectories of components in the VLBI jet of BL Lac. First of all, it is clear that different components follow

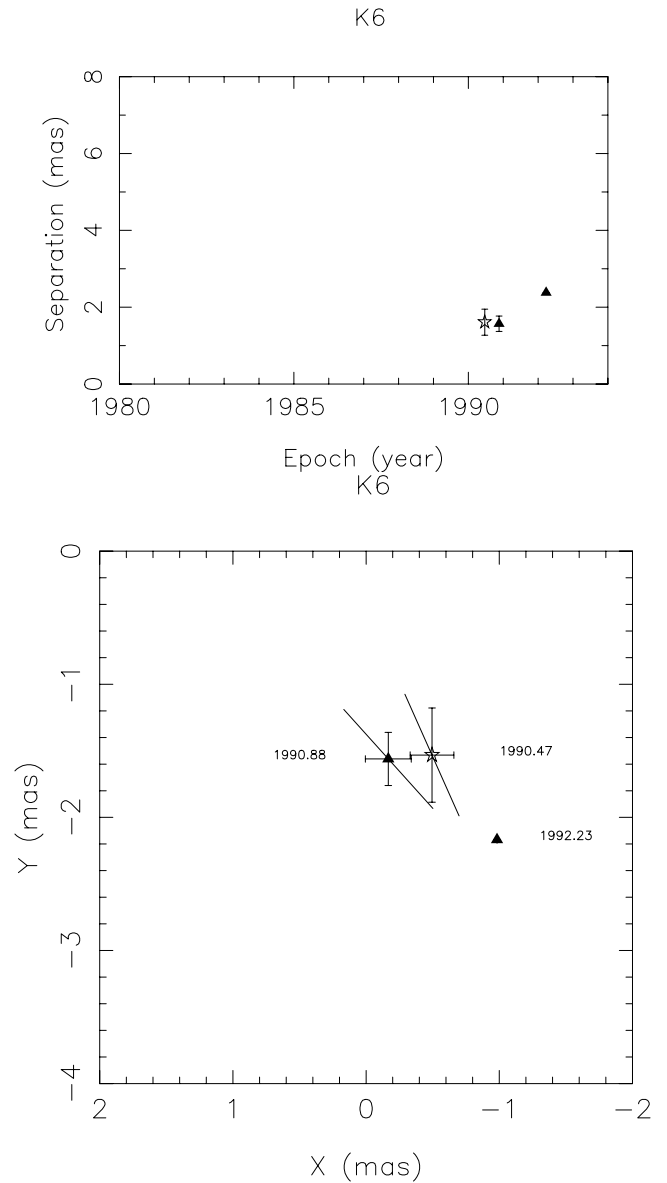


**Figure 10.** (a) Plot of separation from the core versus epoch for our feature K6. (b) Trajectory on the sky of K6. The meaning of the symbols is the same as in Fig. 5. Epochs are indicated next to each of the points. When measured, the orientation of  $\chi$  is shown by a superposed stick (corrected for a foreground rotation measure of  $-108 \text{ rad m}^{-2}$ ). Errors are  $2\sigma$ .

appreciably different trajectories, though in some cases they may be similar to each other. Several features move fairly sharply toward the south-east after separating from the core in position angle roughly  $-170^\circ$ , but the distance from the core where this occurs and details of the movement are different for S1/K1, S2/K2, and S5/K5. The trajectory followed by K3 is quite different, and has not yet shown any tendency to swing toward the south-east at the epoch of our latest image (1992.23); it is even possible that it has begun to move in the opposite direction.

There is also evidence that the measurements of a particular component at different wavelengths trace out slightly different trajectories. For example, for S2/K2, the general impression in Fig. 7(b) is that the 2.8- and 6-cm measurements form a harmonious data set. However, closer inspection shows that, at the three epochs at which

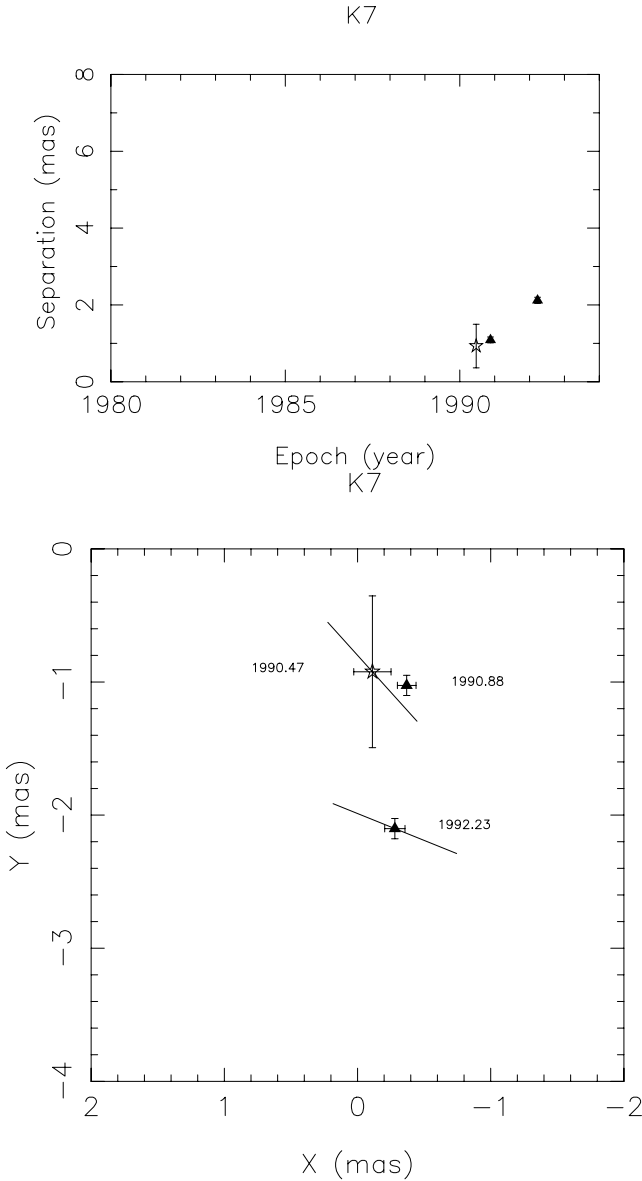


**Figure 11.** (a) Plot of separation from the core versus epoch for our feature K7. (b) Trajectory on the sky of K7. The meaning of the symbols is the same as in Fig. 5. Epochs are indicated next to each of the points. When measured, the orientation of  $\chi$  is shown by a superposed stick (corrected for a foreground rotation measure of  $-108 \text{ rad m}^{-2}$ ). Errors are  $2\sigma$ .

there are nearly simultaneous measurements at 6 and 2.8 cm (within less than two months; 1982.26, 1982.56, and 1983.25 in Fig. 7b), the 2.8-cm positions are always to the west of the 6-cm positions. It is possible that we see this same tendency in Fig. 9(b) for S5/K5, though we do not have enough measurements for this component to be sure of this. The origin of such behaviour is not clear; it may represent a spectral index gradient across the VLBI jet.

In addition, our images suggest that the amplitude of the jet wiggles detected by Mutel et al. (1990) and Denn et al. (2000) within the first  $\sim 2$  mas from the core may become larger with distance from the core. The clearest case is S2/K2 (Fig. 7b). The overall path followed by this feature can be described well by a trajectory that extends in position angle  $\simeq -170^\circ$ , then veers toward the east; however, there are hints that the jet trajectory may deviate slightly

**Table 3.** Apparent component speeds.

Component	Interval	Proper Motion (mas yr $^{-1}$ )	$\beta_{\text{app}}h$
S1/K1	Before 1983.0	1.13	3.51
	After 1984.0	0.67	2.08
S2/K2	Before 1984.0	1.04	3.23
	After 1984.0	0.39	1.21
K3	1983–1993	0.48	1.49
S5/K5	1986–1991	0.48	1.49

eastward about 2–2.5 mas from the core, then turn back westward (near epoch 1986.45) before moving more sharply to the south-east. Similar behaviour may be shown by S1/K1.

## 5 EVOLUTION OF THE POLARIZATION OF OUTFLOWING KNOTS

The results presented here demonstrate that the polarization properties of individual VLBI-scale components can sometimes change rapidly and unpredictably. One example is provided by the results for epochs 1984.23 and 1984.78 in Table 2, which are separated by less than seven months. The total flux densities for the core and the jet knots K3 and S2/K2 measured at the two epochs are nearly the same, and the images are consistent with the polarized flux densities for the core and K3 also being the same. In contrast, the polarized flux for S2/K2 has more than doubled between these two epochs. Since the total intensity of this feature is essentially the same at the two epochs, this represents an increase in its degree of polarization. The origin for this is not clear, though it is interesting that this occurs as it approaches the point where the trajectory for this component bends to the south-east (see Fig. 7b).

Similarly, the feature K3 is modestly polarized in our earlier epochs, but its degree of polarization has risen to nearly 30 per cent at epoch 1987.41, which may correspond to a kink in the jet trajectory, as indicated in Fig. 8(b). In the case of S1/K1, too, we have a substantial increase in the degree of polarization at 1987.41, compared to our earlier epochs.

Fig. 12 summarizes the time evolution of  $I$ ,  $m$ , and  $\chi$  for the four knots for which we have data at more than three epochs (S1/K1, S2/K2, K3, and S5/K5). All three quantities are shown as a function of time on a single plot, in order to make it easier to see how their various behaviours may be correlated. In general, these plots do not show any clear trends or correlations between variations in  $I$ ,  $m$ , and  $\chi$ . For example, some increases in  $I$  may be accompanied by increases in  $m$ , while others clearly are not. In the case of S5/K5, the constancy of the degree of polarization as the total intensity decreases by a factor of 15 is striking (Fig. 12d). Large rotations in  $\chi$  do not generally seem to be accompanied by corresponding changes in  $I$  or  $m$ , consistent with the idea that the changes in  $\chi$  are simply reflecting changes in the direction of that part of the jet through which the component is passing, or a gradual evolution in the jet magnetic field as the components move from the core and expand.

In Figs 6(b)–11(b), we show the directions of the electric vectors for components for which polarization was measured at various epochs; the observed  $\chi$  values were corrected using the foreground rotation measure derived by Reynolds et al. (2001). The behaviour shown in these figures is summarized in Table 4, which indicates whether the intrinsic polarization vector appears to be well aligned

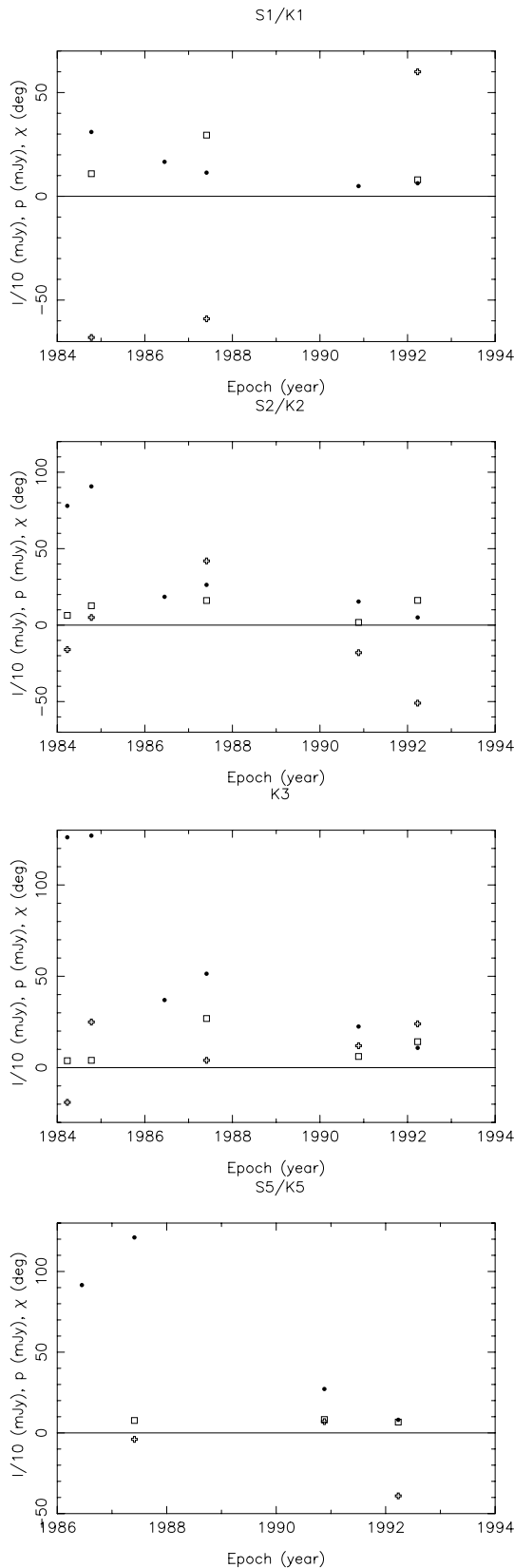


**Figure 12.** Time evolution of the total intensity  $I$  in mJy (filled circles), degree of polarization  $m$  in per cent (squares) and polarization position angle  $\chi$  in degrees (crosses) for components (a) S1/K1, (b) S2/K2, (c) K3 and (d) S5/K5. To enable display of all three quantities simultaneously in a single plot, we show  $I/10$  rather than the full total intensity.

**Table 4.** Polarization alignments.

Component	Epoch	Aligned with Upstream Flow?	Aligned with Downstream Flow?
S1/K1	1984.78	?	Y
	1987.41	$\perp$ ?	Y
	1992.23	$\perp$ ?	
S2/K2	1984.23	y	y
	1984.78	Y	y
	1987.41	$\perp$	$\perp$
	1990.88	y?	Y
	1992.23	Y	
K3	1984.23	y	Y?
	1984.78	y	Y
	1987.41	y	y
	1990.88	y	y
	1992.23	Y	
S5/K5	1987.41	y	?
	1990.47	Y	y
	1990.88	Y	y
	1992.23	Y	
K6	1990.47	y	y
	1990.88	y	Y
K7	1990.47	y?	y?
	1992.23	$\perp$	

Y = well aligned (within  $\simeq 20^\circ$ ); y = roughly aligned ( $20\text{--}35^\circ$ );  $\perp$  = polarization vector transverse to probable flow direction.

$\chi$  values have been corrected for a foreground rotation measure of  $-108$  rad  $\text{m}^{-2}$ .

(within  $\simeq 20^\circ$ ), roughly aligned (within  $20\text{--}35^\circ$ ), or transverse to the upstream and downstream (i.e. toward and away from the core) flows. The information compiled in this table is qualitative, and sometimes uncertain, due to uncertainties in the local flow direction, which we must try to infer from incomplete measurements of component positions as a function of time, and possibly in the foreground rotation measures for individual components. However the table does reflect the general behaviours displayed by polarized features as they move from the core. We consider here these general tendencies, deferring a more detailed analysis of the trajectories of individual components and the relationship of the observed polarization electric vectors to these trajectories to a future paper (Reynolds et al. 2003).

Most BL Lacertae objects have shown a tendency for their jet polarization angles to be aligned with the local jet flow direction (Gabuzda et al. 2000), and references therein), implying the associated magnetic field is transverse, since the emitting regions in question are optically thin. This is true of nearly all of the features detected in the images presented here. Different features show somewhat different behaviour. For example, in some features, there may be a tendency for the polarization vector to be better aligned with the direction downstream (S1/K1) or upstream (S5/K5). Overall, the images analysed here show a general tendency for the polarization vectors to be aligned with the local flow direction, sometimes rotating to remain aligned with the flow direction as the jet trajectory bends.

Our collected images also suggest that different components can experience appreciably different polarization-angle evolution as they move from the core. The trajectories of S1/K1, S2/K2, and S5/K5 all show a bend toward the south-east beyond about 3.5–4.0 mas from the core. The locations on the sky of S1/K1 at 1984.78, S2/K2 at 1987.41, and S5/K5 at 1992.23 are similar, being just beyond this bend. While the corresponding  $\chi$  values for S1/K1 and

S5/K5 are in good general agreement, the  $\chi$  for S2/K2 differs from them by roughly  $90^\circ$  (compare Figs 6b, 7b and 9b). This emphasizes the complex nature of the jet flow and the forces acting on it, and suggests that rapid rotations in polarization angle occur in some regions of the VLBI jet, possibly related to bends in the jet flow, as has been observed by Denn et al. (2000) for some features at higher frequencies closer to the VLBI core.

## 6 CONCLUSIONS

Using our 6-cm images at epochs from 1984.23 to 1992.23 together with our earlier results at 3.6 cm (Gabuzda & Cawthorne 1996) and the 6- and 2.8-cm data of Mutel et al. (1990) and Denn et al. (2000), we have been able to follow the  $I$  and  $P$  evolution of several features substantially further from the core than had been possible using only the earlier images. The VLBI jet components in BL Lac follow similar but distinctly different trajectories, in which there are sometimes oscillations whose amplitude may increase with distance from the core. Further monitoring of the  $I$  and  $P$  VLBI structure of this source at moderate centimetre wavelengths could clearly be valuable for studies of the nature of the jet bends/oscillations.

In most components at most epochs, the polarization vector is at least roughly aligned with the local trajectory for that component, implying that the dominant magnetic field is transverse, as is most common in the VLBI jets of BL Lacertae objects. However there are occasionally cases in which the relation between the  $\chi$  vector and the local jet direction is unclear, or the  $\chi$  vector appears to be transverse to the jet direction. We do not know if this represents the presence of genuinely oblique or longitudinal jet magnetic fields, or if we do not have sufficient information to accurately deduce the local jet flow direction for these components at these epochs.

It is clear that the jet components in BL Lac do not evolve in a regular fashion as they propagate outward from the core. We have found evidence that the degree of polarization of individual features can change appreciably on time-scales as short as several months. In addition, the polarization position angle for individual components can also change substantially and rapidly. In some cases, the polarization angle seems to rotate to retain alignment with respect to the local jet direction, but in other cases the origin of relatively rapid rotations is not obvious. There is no obvious correlation between these rotations and large changes in the degree of polarization of jet components.

More detailed modelling of the trajectories of individual VLBI components and their polarization properties and evolution will be presented by Reynolds et al. (2003).

## ACKNOWLEDGMENTS

This work was supported by an American Astronomical Society Henri Chretien International Research Grant and Small Grant (DCG), and by the UK Particle Physics and Astronomy Research

Council (TVC). DCG acknowledges support from the European Commission under IHP Programme (ARI) contract No. HPRI-CT-1999-00045. The National Radio Astronomy Observatory is operated by Associated Universities, Inc., under cooperative agreement with the NSF. We would also like to thank the staff at the participating observatories who made these observations possible. Finally, we are grateful to the referee, Dr Philip Hughes, for useful comments that have enabled us to significantly improve this paper.

## REFERENCES

- Aller H. D., Aller M. F., Latimer G. E., Hodge P. E., 1985, *ApJS*, 59, 513  
 Altschuler D. R., Wardle J. F. C., 1976, *Mem. R. Astron. Soc.*, 82, 1  
 Angel J. R. P., Stockman H. S., 1980, *ARA&A*, 8, 321  
 Antonucci R. R. J., Hickson P., Olszewski E. W., Miller J. S., 1986, *AJ*, 92, 1  
 Brindle C. et al., 1985, *MNRAS*, 214, 619  
 Cawthorne T. V., Wardle J. F. C., Roberts D. H., Gabuzda D. C., Brown L. F., 1993, *ApJ*, 416, 496  
 Cornwell T. J., Wilkinson P. N., 1981, *MNRAS*, 196, 1067  
 Denn G. R., Mutel R. L., Marscher A. P., 2000, *ApJS*, 129, 61  
 Gabuzda D. C., Cawthorne T. V., 1996, *MNRAS*, 283, 759  
 Gabuzda D. C., Cawthorne T. V., Roberts D. H., Wardle J. F. C., 1989, *ApJ*, 347, 701  
 Gabuzda D. C., Pushkarev A. B., Cawthorne T. V., 2000, *MNRAS*, 319, 1109  
 Gabuzda D. C., Wardle J. F. C., Roberts D. H., 1989, *ApJ*, 338, 743  
 Hughes P. A., Aller H. D., Aller M. F., 1989, *ApJ*, 341, 68  
 Impey C. D., Brand P. W. J. L., Wolstencroft R. D., Williams P. M., 1984, *MNRAS*, 209, 245.  
 Kollgaard R. I., 1994, *Vistas Astron.*, 38, 29  
 Kollgaard R. I., Roberts D. H., Wardle J. F. C., Gabuzda D. C., 1992, *AJ*, 104, 687  
 Miller J. S., 1981, *PASP*, 93, 681  
 Miller J. S., French H. B., Hawley S. A., 1978, in Wolfe A., ed., *Pittsburgh Conference on BL Lac Objects*, Univ. Pittsburgh, Pittsburgh, p. 176  
 Mutel R. L., Phillips R. B., Bumei Su., Buccifero R. R., 1990, *ApJ*, 352, 81  
 Pumphrey R. B., Smith A. G., Leacock R. J., Olssen C. N., Scott R. L., Pollock J. T., Edwards P., Dent W. A., 1976, *AJ*, 81, 489  
 Reynolds C., Cawthorne T. V., Gabuzda D. C., 2001, *MNRAS*, 327, 1071  
 Reynolds C., Cawthorne T. V., Gabuzda D. C., 2003, *MNRAS*, submitted  
 Roberts D. H., Gabuzda D. C., Wardle J. F. C., 1987, *ApJ*, 323, 536  
 Roberts D. H., Wardle J. F. C., Brown L. F., 1994, *ApJ*, 427, 718  
 Rudnick L., Jones T. W., 1983, *AJ*, 88, 518  
 Rudnick L., Jones T. W., Edgar B. K., Pedelty J. A., 1984, *AJ*, 89, 316  
 Schmidt M., 1968, *ApJ*, 151, 393  
 Sitko M. L., Schmidt G. D., Stein W. A., 1985, *ApJS*, 59, 323  
 Smith P. S., Balonek T. J., Elston R., Heckert P. A., 1987, *ApJS*, 64, 459  
 Vermeulen R. C., Ogle P. M., Tran H. D., Browne I. W. A., Cohen M. H., Readhead A. C. S., Taylor G. B., Goodrich R. W., 1995, *ApJ*, 452, L5

This paper has been typeset from a  $\text{\TeX}/\text{\LaTeX}$  file prepared by the author.